Towards a multi-segment ambulatory microrobot

Katie L. Hoffman and Robert J. Wood

Abstract— **The design and kinematics of a multi-segment ambulatory microrobot inspired by centipedes is presented. The kinematics of five repeated segments joined by a flexible backbone of rigid links and flexures are described and simulated. The kinematic model was used to guide the design of an individual two degree of freedom segment, which was fabricated using the Smart Composite Microstructures process. Testing and analysis of a suspended segment displayed motion as predicted by the segment model. Multiple segments can be joined to a flexible backbone to create a multi-segment structure capable of a variety of gaits. Due to its modular, multi-legged, and compact design, this robot has the potential to serve as a platform for swarm robotics applications, advance control techniques for ambulatory systems, and inspire batch fabrication of microrobots.**

I. INTRODUCTION

The development of ambulatory microrobots over the past decade has been motivated by search and rescue operations, hazardous environment exploration, and surveillance. Inspired by the biology of cockroaches, researchers at U.C. Berkeley created RoACH, a 2.4 g, autonomous hexapod robot capable of speeds up to one body length per second [1], using the Smart Composite Microstructures (SCM) process. Similarly, the Harvard Ambulatory Microrobot (HAMR), weighing 90 mg with outer dimensions of 17 mm by 23 mm, has demonstrated forward locomotion using the alternating tripod gait essential to statically stable hexapod locomotion [2]. Additional terrestrial microrobots were designed and fabricated, such as a jumping microrobot [3], a two-legged 10.2 mg robot [4], and a shape memory alloy (SMA) actuated microrobot modeled after a worm [5].

While cockroaches can achieve speeds up to 40 body lengths per second [6], centipedes, part of the subphylum myriapoda, are predatory arthropods that display remarkable agility. In particular, the house centipede, *Scutigera Coleoptera*, is considered the most agile, clocking in at around 10 body lengths per second, and preys on insects [7]. The segmented body of the centipede, which generally has two legs per segments and up to 191 segments in some species [8], allows this arthropod to morph to surfaces, curl around ledges and continue motion on the opposite side, and move from horizontal to vertical surfaces without drastic gait alterations. Flexibility also improves speed by allowing an increase in step size. Significant work was done in the 1950's by Manton on the locomotion of many types of centipedes. In general, it was found that to increase speed, centipedes increase the frequency and angle of swing of the leg as well as extending the legs for a larger stride length [7]. The legs of *Scutigera*, at an average of 1.9 cm on an adult, are longer towards the posterior end to allow overlapping of the legs at high speeds but avoid interference with adjacent legs [7]. The body undulations also increase in magnitude as speed increases, which Manton originally thought to be passive and a result of adjacent legs grouping together around one pivot point [7]; however, it was recently found, through the use of electromyograms attached to the lateral flexor muscles of centipedes running on a treadmill, that the waves moving through the centipede body propagate at the same speed as the muscle activity and are therefore actively controlled by the centipede [9]. Studies were also performed on various types of centipedes in which legs were removed and the resulting locomotion of the centipede was analyzed [7]. Due to the large number of legs, there was no noticeable effect on speed or gait, suggesting that a centipede robot could be adaptable to fabrication defects or damages in the field.

Centipedes have been used as a design guide for robots on larger scales. A six segment walking robot 120 cm in length and weighing 25 kg with passive intersegmental joints formed by gears was constructed using four motors per segment to control two legs [10]. Straight and curved walking was demonstrated. Additionally, [11] used a central pattern generator to study the locomotion of a centipede robot with eight segments, each having two degrees of freedom (DOF), with an extra DOF introduced through the intersegmental connections. Centipedes have also served as inspiration for self-configuring modular robots, such as [12] and [13], which consist of segments that can be attached in a multitude of orientations, giving each robot versatility and robustness.

While these robots utilize the segmented body inherent to myriapod locomotion, they are unable to navigate small spaces and be inexpensively produced. On the smaller scale, current microrobots lack the variety of gaits and added stability capable of a multi-legged robot. A low cost, versatile, and robust multi-segment microrobot could serve as a platform for swarm robotics as well as motivate batch fabrication techniques. Given these motivations, a multi-segment ambulatory microrobot with a passively flexible backbone is under development. A kinematic model was created based on the parameterization of adjacent segments, each having two DOF and connected by three flexures. This model can easily be expanded to study the gaits of a robot with an arbitrary number of segments. The flexure bending energy of a five segment robot was studied as a function of time and phase difference between each segment. Using the kinematic model as a design guide and the Smart Composite Microstructures (SCM) process for fabrication [14], an individual segment

The authors are with the School of Engineering and Applied Sciences, Harvard University, Cambridge, MA 02138 khoffman@fas.harvard.edu

of a multi-segment microrobot with bimorph piezoelectric cantilever actuators controlling the stepping and rotational motion of each segment was designed and constructed. Fabrication and testing of one segment displayed motion as predicted by the segment model.

II. KINEMATICS

The centipede microrobot involves repeated segments, each having two legs and two DOF, connected by passive joints. The robot achieves locomotion by lifting one foot of each segment off the ground while keeping the opposite foot grounded. The segment then rotates relative to the remaining segments with the shoulder of the stance, or grounded, foot acting as the pivot point. Upon completion of the rotational motion, the stance foot is lifted from the surface while the swing, or suspended, foot is being placed on the ground. The process is then repeated with the shoulder of the now grounded foot acting as the new pivot point and the segment rotating in the opposite direction. Adjacent segments are connected by three passive joints, created with flexures. Modeling the passive intersegmental flexures, which are short relative to link length, and the pivot point for each segment as pin joints and using Gruebler's equation shows that three flexures between segments are necessary to match the total DOF of the robot to the number of system inputs.

The system inputs are the angle of rotation of each segment relative to an axis perpendicular to the direction of motion, θ_i, numbered beginning with the most posterior segment, the phase difference of a segment relative to the preceding segment, ϕ_i, and the pivot point for each segment, determined by which foot is grounded. Sinusoidal drive signals are used to rotate each segment, and a square wave controls leg stance to swing transition. Therefore, the last segment is rotated first, and the preceding segment begins motion a phase difference of ϕ_i after the last segment, allowing each actuator drive signal to begin at zero volts. This repeats throughout the segmented body until the most anterior segment has begun moving and gross forward motion has been achieved. The motion begins at the posterior end of the robot rather than the anterior segment to avoid the need to pull the robot forward until each segment is activated. Instead, the body is compressed as motion is initiated.

Given the initial body configuration, rotational angles for each segment, and grounded feet, the current body configuration can be determined quasi-statically using a purely kinematic model describing the external segment configuration. The relevant points on each segment are the stance foot position, the swing foot position, and each of the three flexure positions, labeled in Fig. 1. The rotational angles, θ_i, for each segment can be calculated using the internal segment design given the drive signal, actuator properties, and transmission mechanism described in Sec. III. Assuming the initial stance foot position is an input and future stance feet positions can be calculated based on the previous swing foot position at the time of switching, each of these points of interest can be calculated. Using Fig. 1, the swing foot position is given

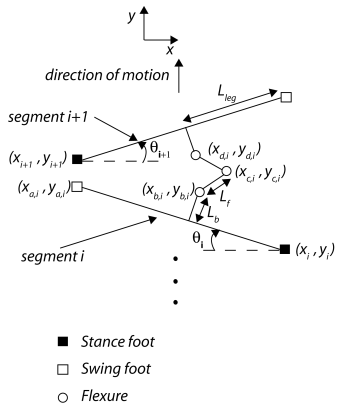

Fig. 1. A kinematic diagram of two segments illustrating the labeling convention for flexure positions, segment rotational angles, and basic segment geometry. Note that each stance foot is also a rotation point.

according to

$$x_{a,i} = x_i + 2L_{leg}\cos\theta_i \tag{1}$$

$$y_{a,i} = y_i + 2L_{leg}\sin\theta_i \tag{2}$$

where L_{leg} is half of the width of a segment and (x_i, y_i) is the stance foot position. The position of the flexure immediately before segment i is only dependent on the angle of rotation and geometry of segment i and is given as

$$x_{b,i} = x_i - L_{leg}\cos\theta_i + L_b\sin\theta_i \tag{3}$$

$$y_{b,i} = y_i + L_{leg}\sin\theta_i + L_b\cos\theta_i \tag{4}$$

where L_b is half of the length of the segment. Similarly, the flexure following segment $i+1$ is only dependent on segment $i+1$:

$$x_{d,i} = x_{i+1} + L_{leg}\cos\theta_{i+1} + L_b\sin\theta_{i+1} \tag{5}$$

$$y_{d,i} = y_{i+1} + L_{leg}\sin\theta_{i+1} - L_b\cos\theta_{i+1} \tag{6}$$

The middle flexure position is dependent on the angles of the surrounding segments:

$$x_{c,i} = x_{b,i} + L_f\cos\eta_i \tag{7}$$

$$y_{c,i} = y_{b,i} + L_f\sin\eta_i \tag{8}$$

where L_f is the length between flexures and η_i is given by

$$\eta_i = \cos^{-1}\frac{x_{b,i} - x_{d,i}}{L_h} - \cos^{-1}\frac{L_h}{2L_f} \tag{9}$$

where

$$L_h = \sqrt{(y_{d,i} - y_{b,i})^2 + (x_{b,i} - x_{d,i})^2} \tag{10}$$

Using these points, it is possible to calculate the amount each flexure is bending according to

$$\gamma_{b,i} = \cos^{-1}\frac{y_{c,i} - y_{b,i}}{L_f} - \theta_i \tag{11}$$

$$\gamma_{c,i} = \cos^{-1}\frac{y_{d,i} - y_{c,i}}{L_f} + \cos^{-1}\frac{y_{c,i} - y_{b,i}}{L_f} \tag{12}$$

$$\gamma_{d,i} = \cos^{-1}\frac{y_{d,i} - y_{c,i}}{L_f} - \theta_{i+1} \tag{13}$$

where $\gamma_{b,i}$, $\gamma_{c,i}$, and $\gamma_{d,i}$ are the angles of rotation for the three flexures between segments i and $i+1$.

For straight line motion, the robot begins in the lowest energy configuration, with each flexure straight and each segment perpendicular to the direction of motion. Motion is initiated with the most posterior segment and adjacent segments begin moving a phase difference later, rotating adjacent segments out of their singular configurations. Subsequent frames of motion from a simulation created using the parameters for the five segment robot discussed in Sec. III for a phase difference of $\pi/2$ for each segment and a driving frequency of 1 Hz are shown in Fig. 2. Flexures between segments are plotted as points, and the stance foot for each segment is shown as a hollow circle. Frames (a) through (f) illustrate the start-up motion of the robot, whereas the last two frames demonstrate the steady state motion.

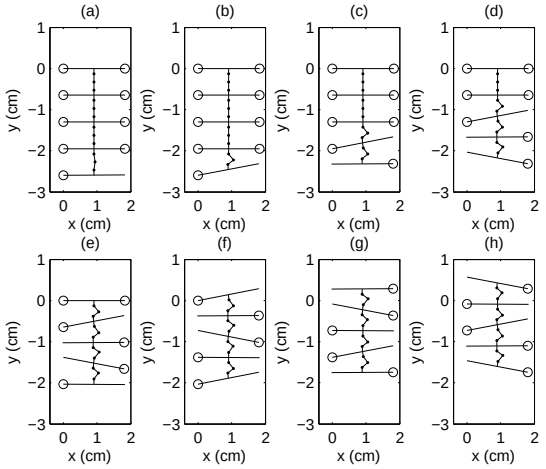

Fig. 2. Simulated straight line motion for a five segment robot with a phase difference of $\pi/2$ between each segment. Points represent flexures between segments, and hollow circles represent the stance foot for each segment. Start up motion is illustrated in (a) through (f), while steady state motion is shown in (g) and (h). Adjacent anterior segments are activated a phase difference of $\pi/2$ after previous segments. Before a segment is activated, both feet on that segment are grounded.

There are multiple observations that can be made based on the kinematic model. By calculating the flexure bending angles at each point in time, it is possible to find the energy stored in the intersegmental flexures at a given time. As a first approximation, this is the minimum amount of work to be done by the actuators to move the body. Neglecting segment inertias and resonance effects and using the kinematic model described above, the flexure bending energy can be calculated as

$$W_i = \frac{1}{2} k \gamma_i^2 \tag{14}$$

where k is the flexure stiffness given by

$$k = \frac{Et^3 w}{12L} \tag{15}$$

E is the modulus of elasticity of the flexure material, t is the thickness, w is the width, and L is the length in the bending direction. Again for a phase difference of $\pi/2$, the flexure potential energy was plotted beginning from the initial motion of the most posterior segment through steady state motion. The result is shown in Fig. 3. The energy increases until steady state is reached after one cycle. The drops in energy during startup occur when the second and fourth segments begin moving, stretching out the flexures and releasing stored energy.

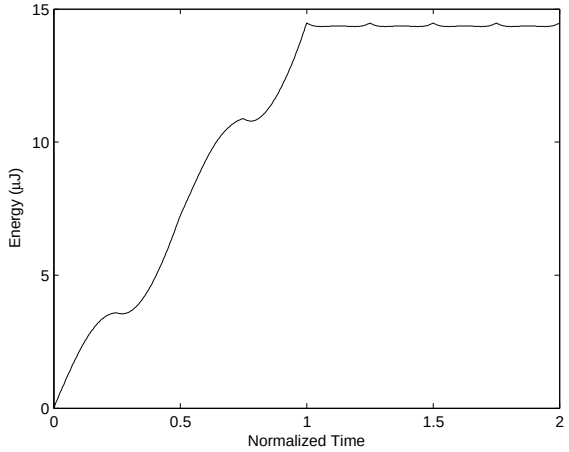

Fig. 3. Flexure bending energy as a function of time normalized to a single cycle for a five segment robot with a phase difference of $\pi/2$ between segments, starting from the lowest energy rest configuration.

In addition to being a function of time, the flexure energy also varies with phase difference. Holding all other parameters constant, the average flexure bending energy at steady state was calculated for a phase difference between segments ranging from $\pi/4$ radians to π radians, with the same phase difference for each of the five segments. For a phase difference of less than $\pi/4$, there is not at least one stance foot on either side of the body, leading to a very unstable body configuration. Instability is defined by having a phase difference of less than $\frac{\pi}{n-1}$ where n is the number of segments. Additionally, phase differences exceeding π, or each segment perfectly out of phase of the previous segment, lead to excessive body compression and potential overlapping of adjacent legs. The average steady state flexure bending energy as a function of phase difference is shown in Fig. 4. The energy steadily increases from a phase difference of $\pi/4$ to a phase difference of just less than π, as the time between the initiation of motion of subsequent segments becomes greater and, therefore, the body is more compressed during motion. At a phase difference of π there is a drastic decrease in the average steady state flexure bending energy as each segment begins motion at the same time, leading to minimal body compression. While it would generally be desirable to minimize flexure bending energy, stability also has to be taken into consideration. For example, the average steady state flexure bending energy for a phase difference of $\pi/4$ is less than that for a phase difference of $\pi/2$; however, the stance foot configuration for a phase difference of $\pi/4$ leads to a less statically stable situation as the legs group

together in a way that causes the first three stance feet to be on the opposite side of the last two stance feet, compared to a phase difference of $\pi/2$, which has the first and last stance feet on the same side and at least one of the middle sets of stance feet on the opposite side forming a stable tripod.

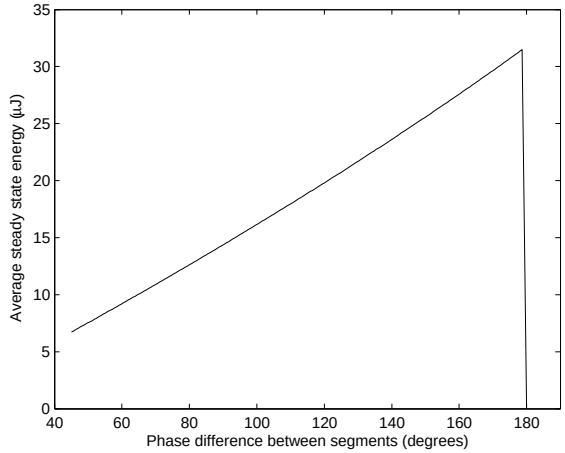

Fig. 4. Flexure bending energy as a function of phase difference for a five segment robot.

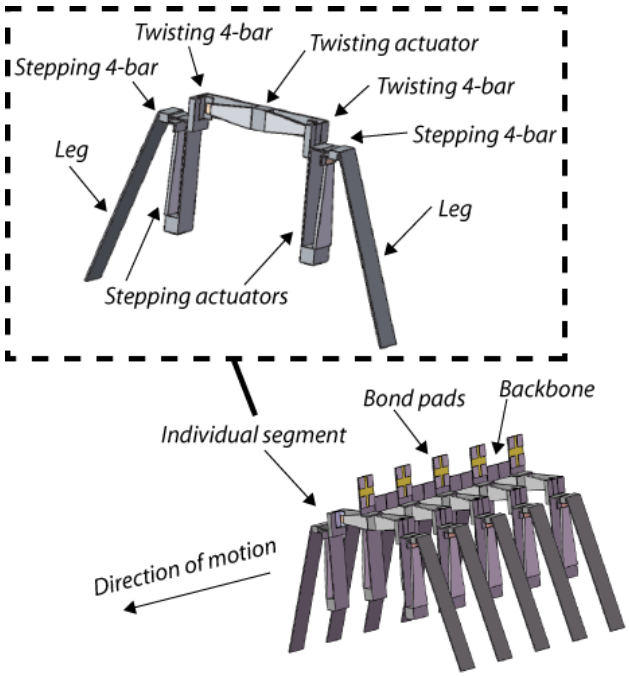

Fig. 5. A concept drawing of a five segment centipede robot highlighting features on both the whole robot and an individual segment.

III. DESIGN

The current design for each individual segment takes into consideration the desired motion based on the external body kinematic model described above, ease of manufacturing, and compactness. Each segment is identical and has two DOF, one that determines which leg is the current pivot point and one that rotates the segment about that pivot point. A rendering of an individual segment is shown in Fig. 5.

The segmental DOF that determines which leg is touching the surface, or the pivot point for that particular segment, is controlled by two bimorph piezoelectric cantilever actuators oriented vertically and parallel to each other. Each actuator provides an approximately linear input to an attached four bar mechanism created using the SCM process described in Sec. IV. The output of the four bar mechanism is a rotational motion, which rotates the leg about an axis parallel to the ground and perpendicular to the width of the segment. A kinematic diagram of this structure is shown in Fig. 6. The bimorphs have opposite poling directions and are coupled by a single drive signal such that when one leg is being lifted, the opposite leg is being placed on the ground. The actuator dimensions are specified using the properties of the piezoelectric and composite materials, trapezoidal geometry, input voltage, and desired maximum force and deflection at the actuator tip, and optimized for energy density using the technique in [15]. The desired actuator tip deflection, δ_1, was determined using a linearized transmission ratio for the four bar mechanism of

$$\alpha_1 \approx T_1 \delta_1 \tag{16}$$

where T_1 is the inverse of the length of the third link in the four bar mechanism, and α_1 is the angle of rotation of the leg. With a transmission ratio of 1/320 rad/μm, determined using a folding technique for SCM structures described in Sec. IV, and an actuator tip deflection of 170 micons peak to peak, the ground clearance is 0.5 mm. Lastly, the legs are attached to the four bar mechanism, angled outward to facilitate leg swing between 5° and 35° measured from the vertical axis.

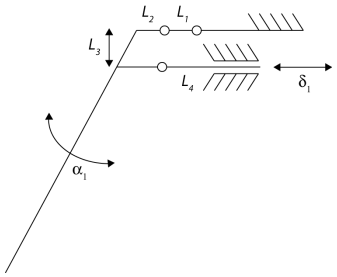

Fig. 6. A kinematic diagram of the mechanism used to determine the stance and swing legs. A linear actuator input δ_1 is transformed into a rotational output α_1 through the use of a four-bar mechanism. The direction of motion of the robot is into the plane of the page.

The mechanism used to rotate segments with respect to ground also utilizes two four bar structures, which are connected to a double bimorph piezoelectric cantilever actuator. These actuators are poled oppositely and have the same drive signal, causing them to deflect in opposite directions. For forward motion, the four bar mechanism attached to the stance leg rotates counterclockwise when viewed from above as the actuator attached to the swing leg moves in the opposite direction, causing the four bar mechanism to also rotate in the counterclockwise direction. When the

legs switch orientation, the actuators also switch direction, causing the now stance leg to rotate clockwise, producing forward motion, while the swing leg resets itself for the next step by also rotating clockwise. A kinematic diagram for this mechanism is shown in Fig. 7. Using the same linearized transmission ratio and kinematics described above for a four bar mechanism, the segmental width, and the distance between adjacent segments, it is possible to calculate the maximum allowable actuator deflection δ_2 for a step size that will not cause interference with adjacent legs according to

$$\delta_2 = T_2 \sin^{-1} \frac{L_f}{L_{leg}} \tag{17}$$

where T_2 is the transmission ratio, and L_f is half the intersegment separation distance when the body is not compressed. Similar to the actuators used for lifting each leg, the width and length of the double cantilever actuator was specified according to the model in [15]. Because the segment width, actuator deflection, and actuator length are not independent, an iterative method was used to find compatible values for these parameters. For a desired step size of 3 mm, a leg length of 9.15 mm, and a transmission ratio of 1/320 rad/μm, the peak-to-peak deflection of the double cantilever actuator was chosen to be 50 μm, giving a maximum body rotation of 9°. The outer dimensions for one segment are 2.5 mm × 21.3 mm × 19 mm.

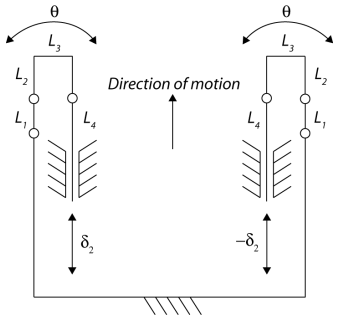

Fig. 7. A kinematic diagram of the mechanism used to rotate an individual segment with respect to the direction of motion. Opposite actuator inputs δ_2 rotate two four-bar mechanisms in the same direction by an amount θ.

The backbone used to connect the segments runs continuously down the center of the body and mounts on top of the support structure for the double cantilever actuator. It incorporates flexures into the body to allow relative motion between segments. The middle flexure between each segment is located 2 mm from the adjacent flexures, while the remaining flexures are located on the anterior and posterior ends of each segment. The height of the backbone was chosen to prevent twisting of the body about an axis parallel to the direction of motion, and the width of the flexures was chosen to allow bending given the torque inputs from the actuators. Bond pads are also integrated into the backbone above each segment to allow wires to attach to an external power source and controller without interfering with the motion of the robot. Two drive signals and one constant high voltage bias signal are necessary to drive one segment. Pictures of the individual mechanisms used to raise and lower the legs and twist the segment and an unattached backbone are shown in Fig. 8.

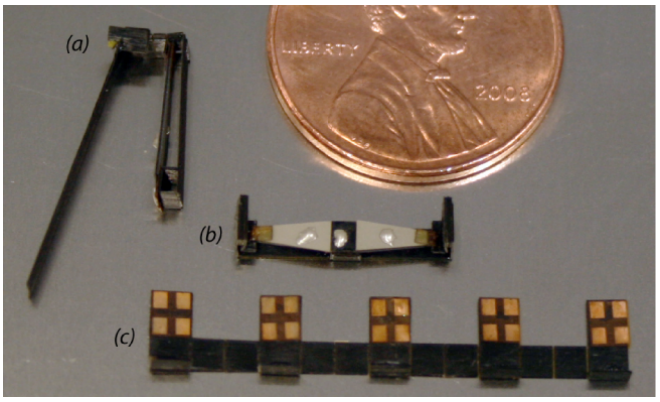

Fig. 8. Completed components for (a) stance control, (b) twisting, and (c) integration (backbone).

IV. FABRICATION

Each segment consists of eight individual pieces which comprise the two subsystems. The components include two transmissions, with attached structures for actuator mounting, for the stepping and twisting motions, legs, and single and double bimorph cantilever actuators. Additionally, one backbone, containing connections for each segment, is necessary. Each of these components is shown in Figure 8. The parts are created using the SCM process [14]. A composite material, in this case a carbon fiber composite prepreg (M60J from Toray), is placed on a tacky substrate (Gelpak). 2D patterns are laser micromachined using a DPSS laser micromachining system, and the excess material is removed. A thin polymer film is placed on top of the composite and also laser machined. A mirror image of the machined composite material is stacked on top of the thin polymer film, and the entire layup is vacuum sealed and cured. Upon removal from the tacky surface, the resulting two dimensional structure can be folded to create a three dimensional structure with flexible joints.

While the last step in this procedure is a manual process, techniques have been developed to reduce the difficulty and manufacturing imperfections resulting from the folding process. This is particularly critical for a multi-legged robot with repeating segments to ensure proper alignment and a reasonable assembly time. To achieve a large transmission ratio for the four-bar components in Fig. 9, it is necessary to make the third link length as small as possible. This can exacerbate fabrication difficulties. To facilitate folding, three 180° folds can be used to create this structure, eliminating the need for a short link. While this requires the third link length, or inverse of the linearized transmission ratio, to be a factor of the thickness of the composite material, in this case, 80 μm, it greatly reduces assembly time and increases yield. A second technique is used to create acute angles for use in the leg orientations. Due to the difficulty in creating

accurate folds at angles other than 180°, alignment tabs were added to the base of the leg structure to ensure accurate folds. As is demonstrated in Fig. 10, a side tab containing a slot equal in width to the thickness of the two dimensional structure and at a 20° angle to the base of the leg structure is folded up perpendicular to the leg, at which point a tab rigidly connected to the leg inserts into the slot.

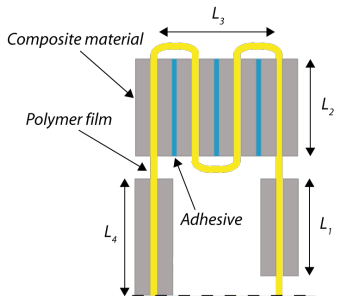

Fig. 9. A diagram of the folding technique used for four-bar mechanisms. Three 180° folds are used to create the third link L_3 in the transmission system.

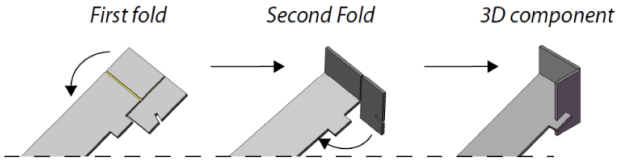

Fig. 10. A diagram of the folding technique used for the legs. A flexible tab containing an angled slot is folded to meet the leg, at which point a rigid tab attached to the leg inserts into the slot.

The actuators are created by layering laser-micromachined carbon fiber prepreg, PZT-5H, and glass fiber prepreg, which provides structural support at the tip of the cantilever in addition to electrical insulation at the base of the actuator. The double cantilever actuators have one continuous layer of carbon fiber and four piezoelectric plates. Wiring is currently done by hand using 50 μm thick wire, chosen to avoid added weight that would affect the motion of the centipede robot. Silver epoxy is used to bond the wire to the piezoelectric material. The four ground and four high voltage plates for the actuators on one segment are wired together as are the drive signals for the two stepping mechanism actuators. These four wires are then soldered to the bond pads attached to the backbone, and, for each segment, four wires are taken from the bond pads on the top of the robot, reducing interference with the moving legs. The bonds pads are created by etching copper-coated polyimide sheets and cured to the backbone.

Upon folding individual components, each segment is assembled and adhered to the backbone. The modular nature of the body as well as the use of a thermoplastic to attach segments allows segments to be added and removed easily. This makes it simple to increase or decrease the number of segments to study different gaits or replace damaged segments throughout the lifetime of the robot without sacrificing the entire system. An individual segment weighs 185 mg and is shown in Fig. 11.

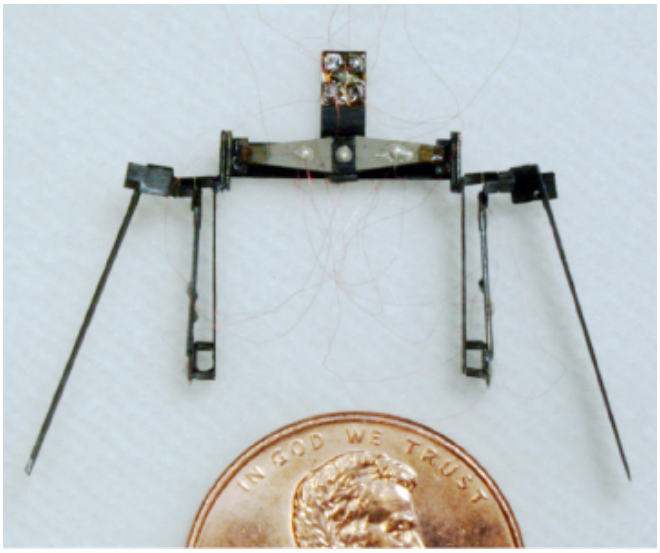

Fig. 11. Assembled Segment.

V. RESULTS

To experimentally validate the segmental design, one segment was constructed and tested. An xPc Target system and high voltage amplifiers were used to control the segment. The segment was suspended and driven at 0.5 Hz at 0 to 200 V. The resulting motion was captured at 20 fps.

The twisting angles were measured with respect to an axis perpendicular to the body. Shown in Fig. 12a, the experimental values are comparable to the predicted value. Fig. 12b shows the experimental results from the stepping mechanism. The legs are expected to rotate from 5° to 35°, switching from being the stance leg to the swing leg, respectively. The experimentally measured angles in Fig. 12b match those predicted by the segmental kinematics, which take into consideration the actuator model and four-bar mechanisms. Subsequent video frames showing the motion of one segment are shown in Fig. 13. The robot begins in the rest state, lifts the right leg and rotates in the second and third frames, respectively, lowers the left leg while lifting the right leg in the fourth frame, rotates in the opposite direction in the fifth frame, and begins to repeat this entire sequence in the sixth frame.

For the purposes of examining integration difficulties, five segments were constructed and bonded to a backbone. This prototype is shown in Fig. 14. Current efforts are geared towards generating locomotion using a similar device.

VI. CONCLUSIONS AND FUTURE WORK

The design and kinematics of a segmented centipede-style microrobot is presented. Identical segments, each having two legs and two DOF can be attached to a flexible backbone to form a multi-segment microrobot capable of locomotion described by the kinematic model presented here. The motion

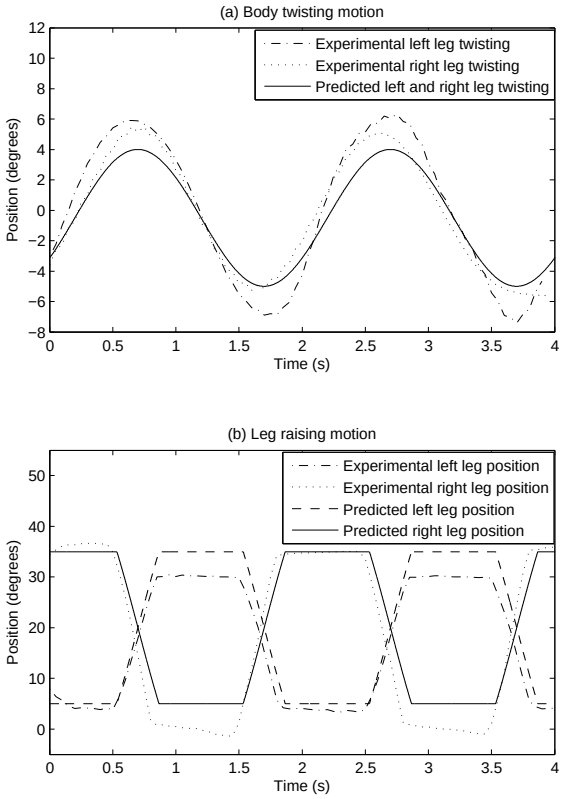

Fig. 12. Predicted and experimental values for the (a) leg rotation about the vertical axis in plane of net body motion and (b) leg rotation about axis parallel to direction of motion.

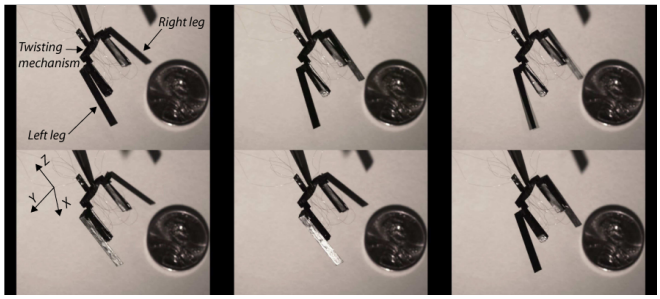

Fig. 13. Video frames showing the motion of one segment.

of one suspended segment was predicted and experimentally tested. Future work will involve verifying the multi-segment kinematic model with a five segment microrobot exhibiting the design presented here as well as advances in batch fabrication of segments, including integrated circuits to decrease wiring time and more automated layering, folding, and assembly techniques. A power source and controller will be housed in each segment to eliminate wires going to an external power source and controller. Additionally, a dynamic model will be created to predict locomotion near resonance and optimize the current design parameters, such as actuator dimensions, segment geometry, and intersegmental flexure stiffness. A versatile multi-segment microrobot modeled after

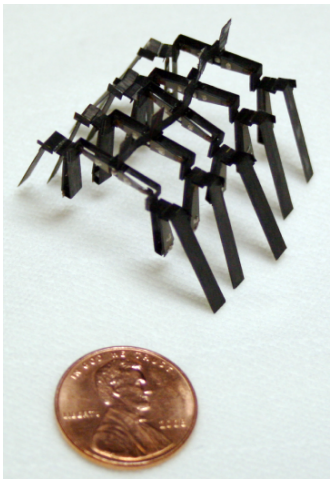

Fig. 14. Prototype of five segment centipede robot.

a centipede will advance the areas of batch microfabrication, control of multi-legged robot locomotion, and algorithm design for decentralized multi-agent systems.

REFERENCES

[1] A. Hoover, E. Steltz, and R. Fearing, "RoACH: An autonomous 2.4 g crawling hexapod robot," in *IEEE/RSJ International Conference on Intelligent Robots and Systems*, 2008, pp. 26–33.

[2] A. Baisch and R. Wood, "Design and fabrication of the harvard ambulatory microrobot," in *14th Int. Symp. of Robotics Research*, 2009.

[3] S. Bergbreiter and K. Pister, "Design of an autonomous jumping microrobot," in *Proc. IEEE International Conference on Robotics and Automation (ICRA07)*, 2007, pp. 10–14.

[4] S. Hollar, A. Flynn, C. Bellew, and K. Pister, "Solar powered 10 mg silicon robot," in *IEEE The Sixteenth Annual International Conference on Micro Electro Mechanical Systems, 2003. MEMS-03 Kyoto*, 2003, pp. 706–711.

[5] B. Kim, M. Lee, Y. Lee, Y. Kim, and G. Lee, "An earthworm-like micro robot using shape memory alloy actuator," *Sensors & Actuators: A. Physical*, vol. 125, no. 2, pp. 429–437, 2006.

[6] R. Full and M. Tu, "Mechanics of a rapid running insect: two-, four- and six-legged locomotion," *J. Exp. Biol.*, vol. 156, pp. 215–231, 1991.

[7] S. Manton and M. Harding, "The evolution of Arthropodan locomotory mechanisms - Part 3. The locomotion of the Chilopoda and Pauropoda," *Journal of the Linnean Society of London, Zoology*, vol. 42, no. 284, pp. 118–167, 1952.

[8] G. Edgecombe and G. Giribet, "Evolutionary biology of centipedes (Myriapoda: Chilopoda)," *The Annual Review of Entomology*, 2006.

[9] B. Anderson, J. Shultz, and B. Jayne, "Axial kinematics and muscle activity during terrestrial locomotion of the centipede Scolopendra heros," pp. 1185–1195, 1995.

[10] A. Torige, S. Yagi, H. Makino, T. Yagami, and N. Ishizawa, "Centipede type walking robot (CWR-2)," in *Proceedings of the 1997 IEEE/RSJ International Conference on Intelligent Robots and Systems*, vol. 1, 1997.

[11] L. Matthey, L. Righetti, and A. Ijspeert, "Experimental study of limit cycle and chaotic controllers for the locomotion of centipede robots," in *IEEE/RSJ International Conference on Intelligent Robots and Systems*, 2008, pp. 1860–1865.

[12] M. Yim, D. Duff, K. Roufas, Y. Zhang, and C. Eldershaw, "Evolution of PolyBot: A Modular Reconfigurable Robot," in *Proc. of the Harmonic Drive Intl. Symposium, Nagano, Japan, Nov*, 2001.

[13] D. Miner, J. Glaros, and T. Oates, "Self-Configuring Modular Centipede Robot," 2007.

[14] R. Wood, S. Avadhanula, R. Sahai, E. Steltz, and R. Fearing, "Microrobot design using fiber reinforced composites," *Journal of Mechanical Design*, vol. 130, p. 052304, 2008.

[15] R. Wood, E. Steltz, and R. Fearing, "Optimal energy density piezoelectric bending actuators," *Sensors & Actuators: A. Physical*, vol. 119, no. 2, pp. 476–488, 2005.